A Hybrid PSO-UKF Framework for Accurate State-of-Charge Estimation in Metal Hydride Hydrogen Tanks

1st Amina YAHIA
UTBM,CNRS, FEMTO-ST, FCLAB
Université Marie et Louis Pasteur
F-90000 Belfort, France
amina.yahia@utbm.fr

2nd Djafar CHABANE
UTBM,CNRS, FEMTO-ST, FCLAB
Université Marie et Louis Pasteur
F-90000 Belfort, France
djafar.chabane@utbm.fr

3rd Salah LAGHROUCHE
UTBM,CNRS, FEMTO-ST, FCLAB
Université Marie et Louis Pasteur
F-90000 Belfort, France
salah.laghrouche@utbm.fr

4th Abdoul N'DIAYE
UTBM,CNRS, FEMTO-ST, FCLAB
Université Marie et Louis Pasteur
F-90000 Belfort, France
abdoul-ousman.n-diaye@utbm.fr

5th Abdesslem DJERDIR
UTBM,CNRS, FEMTO-ST, FCLAB
Université Marie et Louis Pasteur
F-90000 Belfort, France
abdesslem.djerdir@utbm.fr

***Abstract*—Metal hydride hydrogen tank (MHHT) presents a promising approach for achieving safe and environmentally sustainable hydrogen storage, particularly in embedded systems such as electric vehicles. Precise monitoring of the hydrogen content is critical for operational safety; however, direct measurement of the stored hydrogen remains a significant challenge. This work proposes a novel approach for estimating the state-of-charge (SoC) of an MHHT using a custom-developed model in MATLAB and integrating an unscented Kalman filter (UKF) for state estimation. Real-time pressure and temperature measurements are used to validate the accuracy of the UKF-based SoC estimation. To further enhance the filter's performance and robustness, a particle swarm optimization (PSO) algorithm is employed to optimize UKF hyperparameters. The results demonstrate that the hybrid PSO-UKF framework offers a viable and precise method for real-time SoC estimation in MHHTs, achieving RMSE values of 5.1862×10^{-5} and 6.1445×10^{-5} at hydrogen flow rates of 4 and 8 Nl/min, repectively.**

***Index Terms*—Metal hydride hydrogen tanks, SoC, UKF, PSO**

I. Introduction

Green hydrogen, produced by water electrolysis, is of tremendous interest. It is generated from renewable energy and transformed back into power via fuel cells. However, the problem is to effectively store hydrogen for future use. Current storage technologies include compressed gas, liquid cryogenic fluid, and solid metal hydride [1]. Among these, metal hydride storage is promising due to its ability to achieve high hydrogen densities at moderate temperatures and pressures, making it ideal for automotive applications due to its low critical weight penalty [2].

Controlling the hydrogen stored in an MHHT, defined as the state of charge (SoC), is particularly challenging in real-time applications such as vehicles. As hydrogen reacts with the metal alloy to form hydrides, its injected amount can be measured by a flow meter to estimate the SoC through time integration. However, this method has limitations under dynamic conditions, as demonstrated by Suarez et al. [3], where it does not take into account the variability of the internal characteristics of the tank, in addition to the presence of sensor noise that leads to cumulative errors when integrating. Another alternative method is proposed by Chabane et al. [4], by using a piezoelectric ZnO layer on the inner walls of the tank to convert pressure-induced mechanical stress into a voltage output that reflects hydrogen concentration. However, this technique is limited by its reliance on only small deformation assumptions. More advanced approaches use data-driven techniques, such as machine learning and neural networks, to estimate SoC with greater precision. For instance, Collantes et al. [5] developed neural network architectures to estimate SoC in the MHHT using experimental data, but their heavy reliance on high-quality data limits generalization and requires calibration. Zhu et al. [6] developed an online method to estimate SoC for MHHT, combining a Pressure-Composition-Temperature (P-C-T) statistical model with a joint multiclassifier. However, this method is computationally demanding due to the large datasets required for training. Another class of estimators relies on dynamic models of the MHHT to derive the SoC. For example, Alicia et al. [7] introduced an ADRC framework based on a detailed state-space model and an extended state observer. While effective, this approach can be difficult to implement in real time due to its complexity and high computational cost under dynamic conditions.

SoC estimation for MHHTs remains challenging. To address that, an adapted approach is proposed, applying Kalman filtering commonly used in battery systems to the nonlinear MHHTs [8]. Recognizing that the extended Kalman filter (EKF) [9] relies on a Jacobian matrix for linearization, which

is a method that is often inadequate for capturing the strong nonlinearities in MHHTs, the unscented Kalman filter (UKF) [10] is adopted, which employs the unscented transformation for more robust state estimation. In this study, the dynamics of the MHHT are first analyzed and its internal states are estimated via the UKF, from which the SoC is deduced. Furthermore, to overcome the complex and time-consuming process of tuning UKF hyperparameters, a particle swarm optimization (PSO) algorithm is integrated to enhance overall estimator performance. The resulting hybrid PSO-UKF framework is described and validated through simulations of an MHHT operating in the charging phase.

II. Metal Hydride Hydrogen Tank Model

This study analyzes hydrogen behavior in a 0.6 m long, 0.13 m outer, and 0.11 m inner hydrogen storage tank with 11.5 kg of metal alloy. A JULABO FP 52 refrigerated/heating circulator ensures temperature regulation during hydrogen absorption and desorption cycles, maintaining the necessary thermal conditions for system operation.

Before describing the different behaviors of the tank mathematically, few assumptions must be settled in order to reduce the complexity of the modeling [11]:

- Hydrogen gas is ideal.
- Physical characteristics of the metal hydride, such as thermal conductivity, porosity, and volume, remain constant.
- The entire tank and metal hydride have the same temperature.
- Heat convection inside the tank, temperature dependence of thermo-physical values, and radiative transfer in a porous medium are ignored.
- Heat transfer coefficients are assumed constant.

The mathematical model of the MHHT described in this paper is presented in state-space form in order to facilitate the implementation of UKF. The input vector, U, is given by:

$$U = [u] = [\dot{m}_{H_2}] \tag{1}$$

Such that $\dot{m}_{H_2}$ represents the hydrogen flow rate that is injected/rejected to/from the MHHT. The state vector, X, is defined as:

$$X = \begin{bmatrix} x_1 \\ x_2 \\ x_3 \end{bmatrix} = \begin{bmatrix} T_{MH} \\ \rho_g \\ \rho_s \end{bmatrix} \tag{2}$$

Where T_{MH} is the temperature of the metal hydride, ρ_g is the density of hydrogen gas and ρ_s is the density of the metal hydride. The output vector, Y, is set to be:

$$Y = \begin{bmatrix} y_1 \\ y_2 \end{bmatrix} = \begin{bmatrix} P_g \\ T_{w_{out}} \end{bmatrix} \tag{3}$$

Where P_g is the pressure of the hydrogen gas, and $T_{w_{out}}$ represent the temperature of the exiting coolant.

The computation of the three states is directly related to the sorption kinetic k_r; which strongly depends on the thermodynamic conditions of the MHHT, given by:

$$k_r = \begin{cases} C_a e^{\frac{-E_a}{x_1 R}} \ln\left(\frac{P_g}{P_{eq}}\right)(\rho_{ss} - x_3) & ; \quad P_g > P_{eq} \\ C_d e^{\frac{-E_d}{x_1 R}} \left(\frac{P_g - P_{eq}}{P_{eq}}\right)(\rho_{ss} - \rho_0) & ; \quad P_g \leq P_{eq} \end{cases} \tag{4}$$

C_a and C_d are the absorption and desorption constants, respectively, E_a and E_d are the activation energies for absorption and desorption, respectively, R is the gas constant, ρ_{ss} is the density of the saturated metal alloy after it has fully absorbed all gaseous hydrogen that it can reversibly desorb; whereas ρ_0 is the density of the metal alloy after it has desorbed all hydrogen. P_{eq} is the equilibrium pressure.

Assuming that the hydrogen gas is ideal, P_g in the tank obey the following equation:

$$P_g = \frac{R x_2 x_1}{M_{H_2}} \tag{5}$$

Where M_{H_2} is the molar mass of hydrogen. The equilibrium pressure is provided by the pressure-composition-temperature (PCT) curve which represents the interrelationship among pressure, hydrogen concentration in the solid phase and temperature. Once the PCT curve is determined experimentally, P_{eq} can be taken in the central of the plateau of the PCT curve, using this equation:

$$P_{eq} = \left[\sum_{i=1}^{13} p_i \cdot (wt\%)^{13-i}\right] e^{\frac{-|\Delta H|}{R}\left(\frac{1}{x_1} - \frac{1}{T_{ref}}\right)} \tag{6}$$

Where ΔH is the enthalpy (heat) of the reaction, $wt[\%]$ represents the gravimetric storage capacity at the reference temperature T_{ref}, given by this equation:

$$\text{wt}\% = 100 \cdot \frac{\left(\frac{H}{M}\right) M_{H_2}}{M_{MH} + \left(\frac{H}{M}\right) M_{H_2}} \tag{7}$$

where M_{MH} represents the molar mass of metal hydride. $(\frac{H}{M})$ is the hydrogen to metal ratio, given by:

$$\left(\frac{H}{M}\right) = \frac{2(x_3 - \rho_0) M_{MH}}{\rho_0 M_{H_2}} \tag{8}$$

For the coefficients p_i, they are determined by fitting the PCT curve obtained from the experimental tests performed by Chabane et al. in [12].

From (4) to (8), the state space representation of the states can be set as:

$$\begin{bmatrix} \dot{x}_1 \\ \dot{x}_2 \\ \dot{x}_3 \end{bmatrix} = \begin{bmatrix} \dot{T}_{MH} \\ \dot{\rho}_g \\ \dot{\rho}_s \end{bmatrix} = \begin{bmatrix} \dfrac{\left(Q + k_r \frac{\Delta H}{M_{H_2}}\right)}{\varepsilon x_2 c_{pg} + (1-\varepsilon) x_3 c_{ps}} \\ \left(\dfrac{1}{\frac{V_{tank}}{V_{MH}} - 1 + \varepsilon}\right)\left(\dfrac{u}{V_{MH}} - k_r\right) \\ \dfrac{1}{1-\varepsilon} k_r \end{bmatrix} \tag{9}$$

The constants are: ε is the porosity of the metal alloy. C_{pg} and C_{ps} are the specific heat of the gas and solid phases respectively. V_{tank} is the volume of the tank calculated as:

$$V_{tank} = \pi \times \left(\frac{D - de}{2}\right)^2 \times L \tag{10}$$

Where D and L are the external diameter and the length of the internal exchanger of the tank, respectively, and de is the exit port diameter of the tank. For V_{MH}, it represents the volume occupied by the metal alloy, which is 70% of V_{tank}.

Q represents the heat exchanged by the Julabo system to restore the MHHT's equilibrium temperature, and is expressed as:

$$Q = \frac{\dot{m}_w c_{pw}}{V_{MH}}(T_{win} - x_3)\left(1 - e^{\frac{-U\pi DL}{\dot{m}_w c_{pw}}}\right) \tag{11}$$

Where $\dot{m}_w$ is water flow rate, C_{pw} is the specific heat of the water, $T_{w_{in}}$ is the temperature of the entering coolant water coming from the heat exchanger that is fixed at 21°C, U is the global heat transfer coefficient.

Hence, to determine the temperature of the external water circulator $T_{w_{out}}$, the following equation is established:

$$T_{w_{out}} = x_1 + (T_{win} - x_1) \cdot e^{\frac{-U\pi DL}{\dot{m}_w c_{pw}}} \tag{12}$$

The output vector then can be expressed in state space form as:

$$\begin{bmatrix} y_1 \\ y_2 \end{bmatrix} = \begin{bmatrix} \frac{Rx_2x_1}{M_{H_2}} \\ x_1 + (T_{win} - x_1) \cdot e^{\frac{-U\pi DL}{\dot{m}_w c_{pw}}} \end{bmatrix} \tag{13}$$

The previous equations are implemented in Matlab script and solved using ODE45 solver.

The study uses state estimation techniques to infer the hydrogen state-of-charge in MHHT, focusing on pressure and temperature due to their practical advantages and greater measurement reliability, as illustrated in Fig. 1 and Fig. 2.

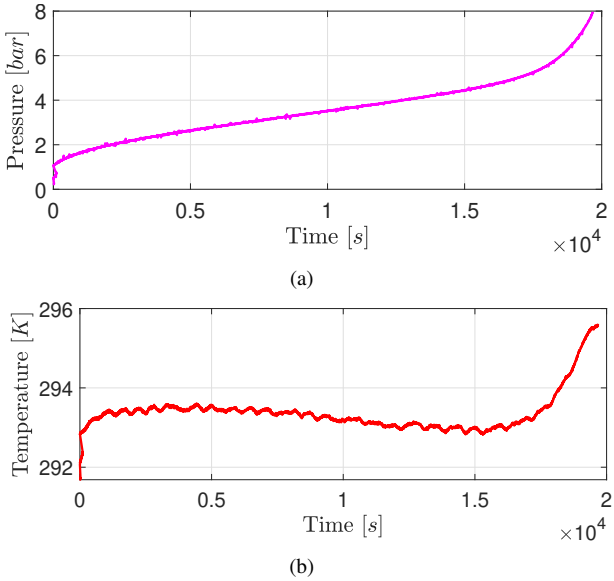

Fig. 1: Pressure and temperature profiles for $\dot{m}_{H_2} = 4$ $[Nl/min]$

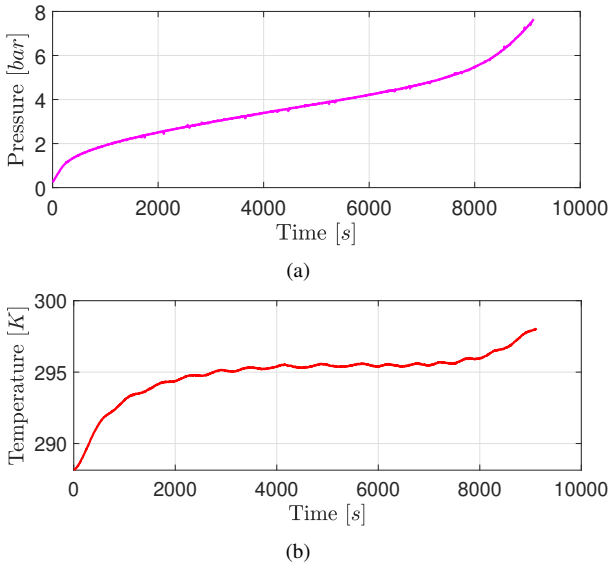

Fig. 2: Pressure and temperature profiles for $\dot{m}_{H_2} = 8$ $[Nl/min]$

For a more comprehensive understanding of the dynamic model of the MHHT, the detailed formulations of (4) – (8) and (10) – (12) can be found in [1], [7] and [11].

III. Unscented Kalman Filter

The Unscented Kalman Filter is a well-known variant of the Kalman Filter family for handling strongly nonlinear systems. As the linear Kalman filter is not suitable for estimation tasks in nonlinear systems such as the MHHT, while the Extended Kalman filter (EKF) treats the non-linearities using analytic linearization via the Jacobian matrix, but still not sufficiently efficient when dealing with strongly non-linear system, the UKF addresses the approximation issues of the EKF by performing the Unscented Transform (UT) [10].

UT provides sigma points that are propagated through the non linear state transition fucntion presented in (9), to predict the state through the nonlinear model. Then, the measurement function presenetd in (13) maps the system states to the sensor outputs, in order to correct the estimation.

This process is outlined in the pseudo-code below [13].

I. Initialisation

- Define control input u, initial state and covariance x_0 and P_0
- Define $f(x) = \texttt{stateTransitionFct}(x, u)$ and $h(x) = \texttt{measurementFct}(x)$
- Define noise covariances Q and R

II. UKF Iteration (For each time step k= 1, ….., N)

1) *Sigma Point Generation:*
   - Generate sigma points $\{\chi_{k-1}\}$ from x_{k-1} and P_{k-1}
2) *Prediction (time update)*
   - Propagate each sigma point: $\bar{\chi}_k = f(\chi_{k-1})$
   - Compute the predicted state: $\hat{x}_k = \sum_i w_i \bar{\chi}_k$
   - Compute the predicted covariance: $P_k^- = \sum_i w_i(\bar{\chi}_k - \hat{x}_k)(\bar{\chi}_k - \hat{x}_k)^T + Q$

3) *Measurement prediction*
   - Transform sigma points into measurement space: $\bar{z}_k = h(\bar{\chi}_k)$
   - Compute the predicted measurement: $\hat{z}_k = \sum_i w_i \bar{z}_k$
   - Calculate the innovation covariance: $S_k = \sum_i w_i(\bar{z}_k - \hat{z}_k)(\bar{z}_k - \hat{z}_k)^T + R$
   - Compute the cross-covariance: $P_{xz,k} = \sum_i w_i(\bar{\chi}_k - \hat{x}_k)(\bar{z}_k - \hat{z}_k)^T$
4) *Correction*
   - Compute the Kalman gain: $\mathbf{K} = P_{xz,k}S_k^{-1}$
   - Update the state estimate with measurement z_k: $\hat{x}_k = \hat{x}_k + \mathbf{K}(z_k - \hat{z}_k)$
   - Update the covariance: $P_k = P_k^- - \mathbf{K}S_k\mathbf{K}^T$

Before initiating the UKF algorithm, several key parameters must be initialized to ensure the proper functioning of the model. In particular, the initial state vector x_0 is defined at $k = 0$ seconds and set as: $x_0 = [294.15, 0.001, 8400]^T$ which represents the starting values of the system states.

The initial state covariance matrix P_0 is typically set based on prior knowledge and is easier to tune manually. In contrast, the process and measurement noise covariances Q and R, which account for system and sensor uncertainties, respectively, are more complex to define due to their variability. Therefore, optimization methods like Particle Swarm Optimization (PSO) are often used to calibrate them effectively.

IV. Particle Swarm Optimization

Particle swarm optimization is an evolutionary computing technique based on random populations that evolved from bird foraging behavior. It involves a swarm of candidate solutions navigating the search space to find optimal solutions by updating their velocities and positions based on their own experiences and neighboring ones [14].

In this work, PSO is employed to optimize the diagonal elements of the noise covariance matrices in the UKF. Each candidate solution is represented as $x = [q_1, q_2, q_3, r_1, r_2, r_3]$, with the process and measurement noise matrices defined as $Q = diag(q_1, q_2, q_3)$ and $R = diag(r_1, r_2, r_3)$, respectively. The performance is evaluated via the root mean square error RMSE, that is the objective function:

$$\text{RMSE} = \frac{1}{N}\sqrt{\sum_{k=1}^{N} \|x_k^{\text{true}} - x_k^{\text{est}}\|^2} \tag{14}$$

Where N is the number of time steps, x_k^{true} is the state computed from the state transition function, and x_k^{est} is the UKF estimate. The PSO algorithm iteratively updates each particle's velocity and position at iteration k using (15) and (16) [15], in order to minimize the RMSE and thereby improves the UKF's performance.

$$v_{id}^k = wv_{id}^{k-1} + c_1 r_1(pbest - x_{id}^{k-1}) + c_2 r_2(gbest - x_{id}^{k-1}) \tag{15}$$

$$x_{id}^k = x_{id}^{k-1} + v_{id}^{k-1} \tag{16}$$

Such that x_{id}^k is the position of the i-th particle of the k-th generation, v_{id}^k is the velocity of the i-th particle of the k-th generation. w is the inertia factor, c_1 is the individual learning factor, whereas c_2 is the social learning factor. $pbest$ and $gbest$ are the particle best position and global best position, respectively. r_1 and r_2 are random numbers between 0 and 1.

V. Results and Discussion

A simulation model was developed using MATLAB to assess the PSO-UKF algorithm's effectiveness in estimating the state of charge of a metal hydride tank. The model constants are listed in Table I.

TABLE I: Model constants

Parameter	Value	Unit
C_a	59.187	$1/s$
E_a	21.1796×10^3	J/mol
R	8.314	$J/mol/K$
ρ_{ss}	8517	Kg/m^3
ρ_0	8400	Kg/m^3
M_{H_2}	2×10^{-3}	Kg/mol
ΔH	30800	J/mol
T_{ref}	294	K
M_{MH}	432.375×10^{-3}	K
ε	0.5	
C_{pg}	14890	$J/Kg/K$
C_{ps}	419	$J/Kg/K$
C_{pw}	2400	$J/Kg/K$
$\dot{m}_w$	0.0033	Kg/s
$T_{w_{in}}$	294	K
U	300	$W/(m^2.K)$
D	0.13	m
L	1.2	m

A. Covariance matrix optimization of UKF

The diagonal elements of the noise covariance matrices Q and R are optimized using the PSO algorithm. The dimensionality of PSO particles is set to 6, and the optimal solution is identified by minimizing the objective function. The final optimized values of Q and R are: $Q = diag([0.5, 0.1, 0.01])$ and $R = diag([0.05, 0.05, 0.01])$.

B. UKF estimation

Case **I***:* After incorporating the optimized values of Q and R into the UKF algorithm and setting the control input to be $4Nl/min$, the obtained results for the predicted states are depicted in Fig. 3 :

Fig. 3 demonstrates that the UKF estimate for temperature, gas density, and solid density closely match the true states from the outset. There is no discernible initial deviation, indicating that the filter was well-initialized and quickly converged, which suggests effective tuning and minimal measurement noise. The simulation time is 4800 s. The overall RMSE evaluated is 5.1862×10^{-5} which reflects the small deviation between true and estimated states.

Since SoC is directly derived from ρ_s by this equation:

$$\text{SoC } \% = \frac{\rho_s^{\text{est}} - \rho_0}{\rho_{ss} - \rho_0} \times 100 \tag{17}$$

The SoC estimation is given in Fig. 4. It can be seen that the estimated SoC closely aligns with the true SoC throughout

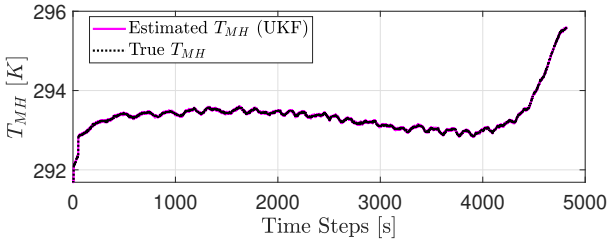

(a) UKF Estimation of Metal Hydride Temperature

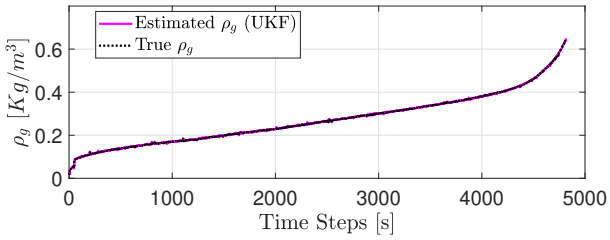

(b) UKF Estimation of Gas Density

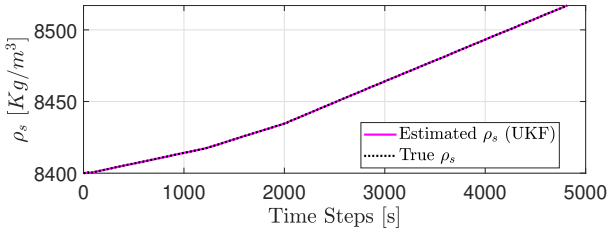

(c) UKF Estimation of Solid Density

Fig. 3: States estimate results.

the time horizon. The SoC error indicates that the difference between the estimated and true SoC remains extremely small (on the order of 10^{-5}), demonstrating that the estimation method is accurate and stable during the absorption process.

Case **II***:* In the second case, the hydrogen flow rate is doubled to show the effect of providing more hydrogen on the state of charge of MHHT.

The results derived from the state estimation are illustrated in Fig. 5, where the UKF estimates converge rapidly to the true states with a control input of $8Nl/min$. Compared to the first case, the estimation time is significantly reduced from 4800 s to 1800 s, demonstrating that a higher hydrogen flow rate speeds up system dynamics and UKF convergence. The low RMSE of 6.1445×10^{-5} further confirms the accuracy and effectiveness of the filter tuning.

As shown in Fig. 6, the estimated SoC closely follows the true SoC, converging quickly with minimal error. A brief mid-simulation peak is observed before the error returns near zero. This demonstrates that higher hydrogen flow accelerates MHHT saturation and confirms the robustness and efficiency of the estimation method under reduced time conditions.

C. Computational Performance of PSO-Based UKF Tuning

Computing time is directly related to the complexity of the estimation framework. In this study, six UKF hyperparameters were tuned offline using PSO. Although PSO ensures reliable

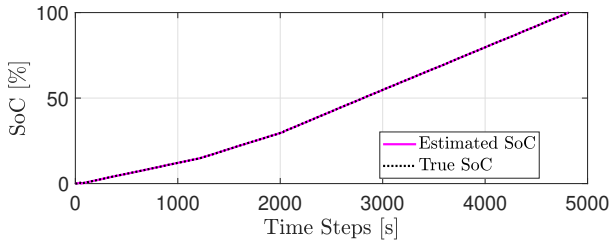

(a) UKF Estimation of MHT state of charge

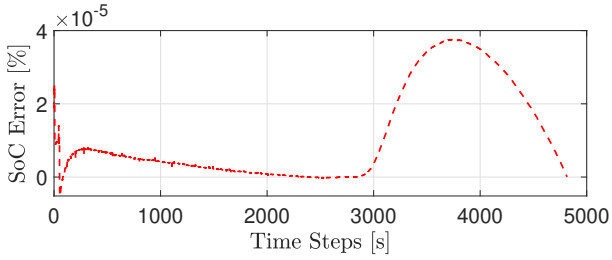

(b) SoC error

Fig. 4: SoC estimation and error.

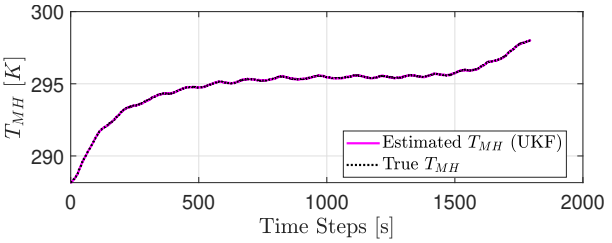

(a) UKF Estimation of Metal Hydride Temperature

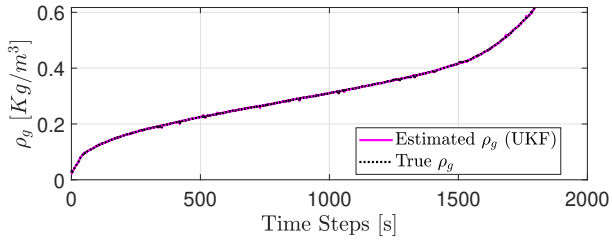

(b) UKF Estimation of Gas Density

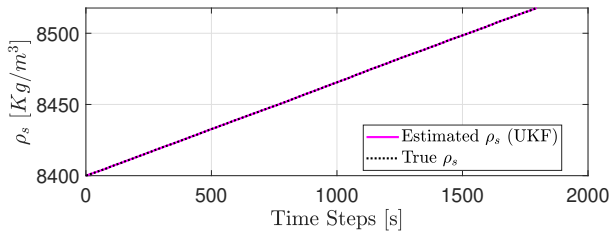

(c) UKF Estimation of Solid Density

Fig. 5: States estimate results.

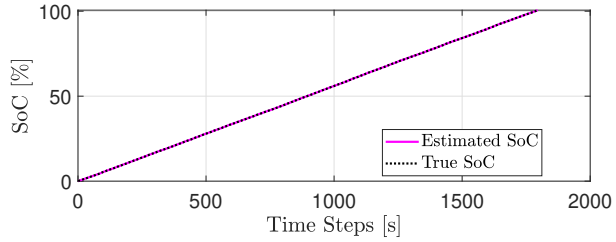

(a) UKF Estimation of MHT state of charge

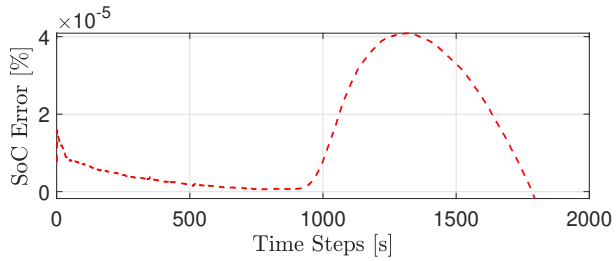

(b) SoC error

Fig. 6: SoC estimation and error.

convergence and effective exploration of how the error changes with different parameter values, its computational cost grows with the number of parameters. Even with a reduced swarm of 20 particles, the calibration phase required approximately 60 minutes of CPU time to reach a satisfactory objective-function minimum, which makes real-time tuning impossible in embedded applications. This expense is, however, strictly confined to the offline stage: once PSO convergence is achieved, the resulting hyperparameters remain fixed and can be applied repeatedly, allowing the UKF to perform rapid, real-time SoC estimation without any additional optimization overhead.

VI. Conclusion

This study proposes a novel estimation method based on a hybrid Particle Swarm Optimization–Unscented Kalman Filter (PSO-UKF) algorithm, which exhibits strong accuracy and robustness. This work presents three main key contributions. First, a specific model of the MHHT was developed and formulated in a nonlinear state-space representation. Then, the UKF was implemented to estimate the SoC of hydrogen within the MHHT. The performance of the UKF was significantly improved by employing the PSO algorithm to optimally tune the process and measurement noise covariance matrices. Finally, the proposed PSO-UKF approach was evaluated using simulated temperature and pressure data, demonstrating its ability to accurately estimate the internal states of the system, therefore the SoC, with low estimation error.

Future work will pursue three main directions. First, the PSO–UKF estimator will be validated experimentally on a real-time MH tank system to confirm its practical performance. Second, strategies for accelerating the offline calibration will be investigated to enhance real-time feasibility by reducing the tuning time. Finally, a comprehensive robustness study will be conducted under varying measurement noise levels, ambient temperature fluctuations, and sensor delays, accompanied by a sensitivity analysis to assess the estimator's stability and adaptability across different operating conditions.

Acknowledgment

This work has been supported by the EIPHI Graduate School (contract ANR-17- EURE-0002) and the Region Bourgogne Franche-Comte within the framework of the ESYSH2 project.

References

[1] D. Chabane, F. Harel, A. Djerdir, D. Candusso, O. Elkedim, and N. Fenineche, "Energetic modeling, simulation and experimental of hydrogen desorption in a hydride tank," *International Journal of Hydrogen Energy*, vol. 44, pp. 1034–1046, 1 2019.

[2] D. Zhu, Y. Ait-Amirat, A. N'Diaye, and A. Djerdir, "New dynamic modeling of a real embedded metal hydride hydrogen storage system," *International Journal of Hydrogen Energy*, vol. 44, pp. 29 203–29 211, 11 2019.

[3] S. H. Suárez, D. Chabane, A. N'Diaye, Y. Ait-Amirat, and A. Djerdir, "Static and dynamic characterization of metal hydride tanks for energy management applications," *Renewable Energy*, vol. 191, pp. 59–70, 5 2022.

[4] N. Fenineche, D. Chabane, L. SERAIRI, O. Elkedim, and A. Djerdir, "Estimation of the state of charge of a hydride tank using piezoelectric materials," 10 2019.

[5] V. Torres Collantes, "State of charge estimation of metal hydride storage tank using neural networks," Ph.D. dissertation, UPC, Escola d'Enginyeria de Barcelona Est, Departament d'Enginyeria de Sistemes, Automàtica i Informàtica Industrial, Jun 2024. [Online]. Available: http://hdl.handle.net/2117/419981

[6] D. Zhu, Y. Ait-Amirat, A. N'Diaye, and A. Djerdir, "On-line state of charge estimation of embedded metal hydride hydrogen storage tank based on state classification," *Journal of Energy Storage*, vol. 42, 10 2021.

[7] A. L. J. Keow, A. Mayhall, M. Cescon, and Z. Chen, "Active disturbance rejection control of metal hydride hydrogen storage," *International Journal of Hydrogen Energy*, vol. 46, pp. 837–851, 1 2021.

[8] P. Shrivastava, T. K. Soon, M. Y. I. B. Idris, and S. Mekhilef, "Overview of model-based online state-of-charge estimation using kalman filter family for lithium-ion batteries," 10 2019.

[9] S. Jiang, J. Shi, M. Borah, and S. Moura, "Weaknesses and improvements of the extended kalman filter for battery state-of-charge and state-of-health estimation," in *2024 American Control Conference (ACC)*, 2024, pp. 1441–1448.

[10] A. Becker, *Kilman filter : from the ground up*. KilmanFilter.NET, 2023.

[11] S. H. Suárez, D. Chabane, A. N'diaye, Y. Ait-Amirat, O. Elkedim, and A. Djerdir, "Evaluation of the performance degradation of a metal hydride tank in a real fuel cell electric vehicle," *Energies*, vol. 15, 5 2022.

[12] D. Chabane, F. Harel, A. Djerdir, D. Candusso, O. ElKedim, and N. Fenineche, "A new method for the characterization of hydrides hydrogen tanks dedicated to automotive applications," *International Journal of Hydrogen Energy*, vol. 41, pp. 11 682–11 691, 7 2016.

[13] E. Wan and R. Van Der Merwe, "The unscented kalman filter for nonlinear estimation," in *Proceedings of the IEEE 2000 Adaptive Systems for Signal Processing, Communications, and Control Symposium (Cat. No.00EX373)*, 2000, pp. 153–158.

[14] R. Boqiang and J. Chuanwen, "A review on the economic dispatch and risk management considering wind power in the power market," pp. 2169–2174, 10 2009.

[15] T. Xie, X. Xu, F. Yuan, Y. Song, W. Lei, R. Zhao, Y. Chang, X. Wu, Z. Gan, and F. Zhang, "Speed estimation strategy for closed-loop control of pmsm based on pso optimized kf series algorithms," *Electronics (Switzerland)*, vol. 12, 10 2023.